Examination of Capacities of Cr-Si_{60}, Cr-C_{60} and Cr-Ge_{60} Nanocages as High Efficiency Catalysts for Oxygen Reduction Reaction (ORR) in Fuel Cell

[1]Ziyan Cheng, [1]Liyan You*, [1]Chaohong Ma and [2]Tiang Hengo
[1]*School of Biological and Pharmaceutical Engineering, JiLin Agricultural Science and Technology College, Jilin, Jilin 132101, China.*
[2]*Shaoxing Hanli Industrial Automation, Shaoxing, Zhejiang, China*.
youliyan@jlnku.edu.cn*

(Received on 30th May 2025, accepted in revised form 20th October 2025)

Summary: Here, the capacities of Cr-Si_{60}, Cr-C_{60} and Cr-Ge_{60} nanocages of ORR are examined. The mechanisms of ORR on Cr-Si_{60}, Cr-C_{60} and Cr-Ge_{60} nanocages as catalysts are investigated. Results indicated that Cr have favorable bonds with Si, C and Ge of Cr-Si_{60}, Cr-C_{60} and Cr-Ge_{60} nanocages. The OOH adsorption on Cr-Si_{60}, Cr-C_{60} and Cr-Ge_{60} nanocages is more favorite process than O_2 dissociation from thermodynamic view point. The *OH formation is rate-determining for ORR on Cr-Si_{60}, Cr-C_{60} and Cr-Ge_{60} nanocages. The Cr-Si_{60}, Cr-C_{60} and Cr-Ge_{60} have higher catalytic activity for ORR processes than metal-based catalysts and AlN, C, BN, AlP and BP nanocages and AlN, C, BN, Si, Ge, AlP and BP nanotubes. The over-potential of ORR on surfaces of Cr-Si_{60}, Cr-C_{60} and Cr-Ge_{60} are lower than metal based catalysts. The Cr-Si_{60} and Cr-Ge_{60} nanocages have lower over-potential for ORR than Cr-C_{60} nanocage. The Cr-Si_{60} and Cr-Ge_{60} are proposed as new catalysts for reaction steps of ORR by acceptable performance.

Keyword: Oxygen-RR, Si_{60}, Nano-catalyst, Reduction mechanism, Acid environment, Over-potential.

Introduction

The oxygen reduction reaction (ORR) can be reduced the efficiency and performance of fuel cells [1]. The one way to increase the efficiency of fuel cells is to reduce the oxygen reduction reaction (ORR). Researchers have made great efforts to find suitable catalysts for the oxygen ORR. The metal-based catalysts have moderate efficiency for the ORR [2]. The metal-based catalysts have low stability and high cost, as well as environmental problems for the ORR [3].

The carbon nanoparticle-based catalysts for the ORR have high stability, low cost, and large surface area [4]. The carbon nanoparticle-based catalysts can improve the efficiency of fuel cells by catalyzing the ORR [5]. The adsorption of metals on the surface of carbon-based catalysts can significantly increase the efficiency of carbon nanoparticle-based catalysts. The metals adsorbed on carbon nanoparticle-based catalysts have the ability to adsorb species related to ORR [6].

In previous works, the capacities of various metal-based catalysts [7] and Metals (Fe, Co, Ni and Cu) doped AlN, C, BN, AlP and BP nanocages and Metals (Fe, Co, Ni and Cu) doped AlN, C, BN, Si, Ge, AlP and BP nanotubes [8] for ORR processes have been examined. The mechanisms for ORR processes on surfaces of various metal-based catalysts [9] and Metal doped nanostructures have been investigated [10]. Results have shown than the Metal doped nanostructures [11] have higher catalytic activity for ORR processes than various metal-based catalysts [12]. Results have indicated that the pathways and their steps of ORR on various metal-based catalysts [13] and Metal doped nanostructures have been investigated [14] are same.

Researcher have demonstrated that the C_{60} structure is one of the most stable nanocages that has high surface area, thermodynamic stability and high catalytic activity for inorganic reactions [15]. The other derivatives of C_{60} structure such as Si_{60} and Ge_{60} structures similar to C_{60} structure have high thermodynamic stability and formation energy and their surfaces area have higher than C_{60} structure. The metal adoption on surfaces of C_{60}, Si_{60} and Ge_{60} structures can improve their catalytic capacities to adsorb the intermediates of important organic reactions [16].

In this study, the potential of Cr-Si_{60}, Cr-C_{60} and Cr-Ge_{60} nanocages of ORR are investigated. The effects of adsorption of Cr on Si_{60}, C_{60} and Ge_{60} on capacities for ORR are examined. The acceptable pathways of ORR on Cr-Si_{60}, Cr-C_{60} and Cr-Ge_{60} are examined. The goals of this work are: to suggest the catalysts (Cr-Si_{60}, Cr-C_{60} and Cr-Ge_{60}) for ORR with acceptable performances; to compare the performances of Cr-Si_{60}, Cr-C_{60} and Cr-Ge_{60} for ORR; to propose available pathways of ORR on Cr-

*To whom all correspondence should be addressed.

Si_{60}, Cr-C_{60} and Cr-Ge_{60}; to find the Cr adsorption effects on capacities of Cr-Si_{60}, Cr-C_{60} and Cr-Ge_{60} for ORR; to compare the efficiency of Cr-Si_{60}, Cr-C_{60} and Cr-Ge_{60} for ORR with metal based catalysts.

Computational details

The geometries of Si_{60}, C_{60}, Ge_{60}, Cr-Si_{60}, Cr-C_{60} and Cr-Ge_{60} and complexes with ORR derivatives have been optimized by M06-2X/6-311+G (2d, 2p) model in GAMESS software [16, 17]. The frequencies of Si_{60}, C_{60}, Ge_{60}, Cr-Si_{60}, Cr-C_{60} and Cr-Ge_{60} and complexes with ORR derivatives are calculated to confirm that the nano-structures are stable structures [18, 19]. The capacities of Cr-Si_{60}, Cr-C_{60} and Cr-Ge_{60} to adsorb of ORR species are examined. The structures of Si_{60}, C_{60} and Ge_{60} nanocages are reported in Figure 1. The $E_{formation}$ of Si_{60}, C_{60} and Ge_{60} are summarized in Figure 1. The possible mechanisms for ORR on Cr-Si_{60}, Cr-C_{60} and Cr-Ge_{60} nanocages are examined to propose the acceptable mechanism and new catalysts with high performances. The ORR on surfaces of Cr-Si_{60}, Cr-C_{60} and Cr-Ge_{60} nanocages is processed by three pathways as presented in Table 1. The $\Delta G_{reaction}$ and $E_{activation}$ of ORR on Cr-Si_{60}, Cr-C_{60} and Cr-Ge_{60} are investigated in Table 1.

Results and discussion

Adsorption of ORR species on Cr-Si_{60}, Cr-C_{60} and Cr-Ge_{60} nanocages

The $E_{formation}$ of Si_{60}, C_{60} and Ge_{60} nanocages are -5.89, -4.42 and -5.58 eV. The $E_{formation}$ of Si_{60} are higher than C_{60} and Ge_{60} nanocages ca 1.52 and 0.31 eV. Results shown that $E_{formation}$ of Si_{60}, C_{60} and Ge_{60} nanocages are negative.

The $E_{formation}$ of Si_{60}, C_{60} and Ge_{60} are calculated as following [19]:

$$E_{formation} = E_{nanocage} - 60 * E_X \quad (1)$$

The $E_{nanocage}$ is total energies of Si_{60}, C_{60} and Ge_{60} nanocages and the E_X are energies of Si, C, Ge atoms. The adoption energies ($E_{adoption}$) of Cr atoms on Si_{60}, C_{60} and Ge_{60} nanocages are calculated as following [20]:

$$E_{adoption} = E_{Cr\text{-}nanocage} - E_{nanocage} - E_{Cr} \quad (2)$$

The $E_{Cr\text{-}nanocage}$ is total energies of Cr-Si_{60}, Cr-C_{60} and Cr-Ge_{60} complexes and the $E_{nanocage}$ is total energies of Si_{60}, C_{60} and Ge_{60} and E_{Cr} is energy of Cr. The $E_{adsorption}$ of ORR derivatives on Cr-Si_{60}, Cr-C_{60} and Cr-Ge_{60} nanocages are calculated as following [21]:

$$E_{adsorption} = E_{specie\text{-}Cr\text{-}nanocage} - E_{Cr\text{-}nanocage} - E_{specie} \quad (3)$$

The $E_{specie\text{-}Cr\text{-}nanocage}$ is energies of complexes of Cr-Si_{60}, Cr-C_{60} and Cr-Ge_{60} nanocages with ORR derivatives, the $E_{Cr\text{-}nanocage}$ is energies of Cr-Si_{60}, Cr-C_{60} and Cr-Ge_{60} nanocages and the E_{specie} is energies of ORR derivatives.

The Cr adoption on Si_{60}, C_{60} and Ge_{60} nanocages are examined and structures of Cr-Si_{60}, Cr-C_{60} and Cr-Ge_{60} are presented in Figure 1. The $E_{adoption}$ of Cr on Si_{60}, C_{60} and Ge_{60} are shown in Figure 1. The $E_{adoption}$ of Si_{60}, C_{60} and Ge_{60} nanocages are -4.56, -4.15 and -4.41 eV. The $E_{adoption}$ of Cr-Si_{60} are more negative than Cr-C_{60} and Cr-Ge_{60} nanocages ca 0.41 and 0.15 eV. The $E_{adoption}$ of Cr on Si_{60}, C_{60} and Ge_{60} are negative and Cr have acceptable bonds with Si, C and Ge of Cr-Si_{60}, C_{60} and Ge_{60} nanocages. The Cr-Si_{60}, Cr-C_{60} and Cr-Ge_{60} are stable structures and Cr is active site for ORR adsorption.

In this section, the adsorption of ORR species on Cr-Si_{60}, Cr-C_{60} and Cr-Ge_{60} are investigated. The structures of complexes of ORR species with Cr-Si_{60}, Cr-C_{60} and Cr-Ge_{60} are shown in Figure 1. The O_2 is joined to Cr of Cr-Si_{60}, Cr-C_{60} and Cr-Ge_{60} nanocages. The $E_{adsorption}$ of O_2 on Si_{60}, C_{60} and Ge_{60} nanocages are -0.45, -0.37 and -0.40 eV. The $E_{adsorption}$ of O on Si_{60}, C_{60} and Ge_{60} nanocages are -3.30, -2.87 and -2.96 eV. The $E_{adsorption}$ of O + O on Si_{60}, C_{60} and Ge_{60} nanocages are -6.54, -5.78 and -5.87 eV.

The O + O and O have high interactions with Cr of Cr-Si_{60}, Cr-C_{60} and Cr-Ge_{60} and have acceptable $E_{adsorption}$. The O_2 on Cr-Si_{60}, Cr-C_{60} and Cr-Ge_{60} nanocages is produced the O and O + O on Cr of Cr-Si_{60}, Cr-C_{60} and Cr-Ge_{60} nanocages. The $E_{adsorption}$ values of O + O and O with Cr-Si_{60}, Cr-C_{60} and Cr-Ge_{60} are higher than O_2. The OH and OOH are adsorbed on Cr atoms of Cr-Si_{60}, Cr-C_{60} and Cr-Ge_{60} nanocages and $E_{adsorption}$ are higher than O_2. The Cr-Si_{60}, Cr-C_{60} and Cr-Ge_{60} have higher capacities for ORR species adsorption than OH and OOH. The H_2O on Cr-Si_{60}, Cr-C_{60} and Cr-Ge_{60} are physically absorbed and H_2O is easily desorbed from Cr-Si_{60}, Cr-C_{60} and Cr-Ge_{60} nanocages. The $E_{adsorption}$ of ORR species on Cr-Si_{60} and Cr-Ge_{60} nanocages are higher than Cr-C_{60} nanocage.

In this study, the E_{HLG} and q as charge transfer of Cr-Si_{60}, Cr-C_{60} and Cr-Ge_{60} nanocages and complexes of Cr-Si_{60}, Cr-C_{60} and Cr-Ge_{60} with ORR species are reported in Table 2. The complexes of ORR species (O, OH, OOH, O + O and H_2O) on Cr-Si_{60} have lower E_{HLG} than corresponding values for Cr-C_{60} and Cr-Ge_{60}

nanocages. The q as charge transfer between the ORR species (O, OH, OOH, O + O and H_2O) and Cr-Si_{60} have higher corresponding values for Cr-C_{60} and Cr-Ge_{60} nanocages. The Cr-Si_{60} and Cr-Ge_{60} have higher capacities to join with ORR species than Cr-C_{60}. The Cr-Si_{60} and Cr-Ge_{60} nanocages have higher potential than Cr-C_{60} for ORR.

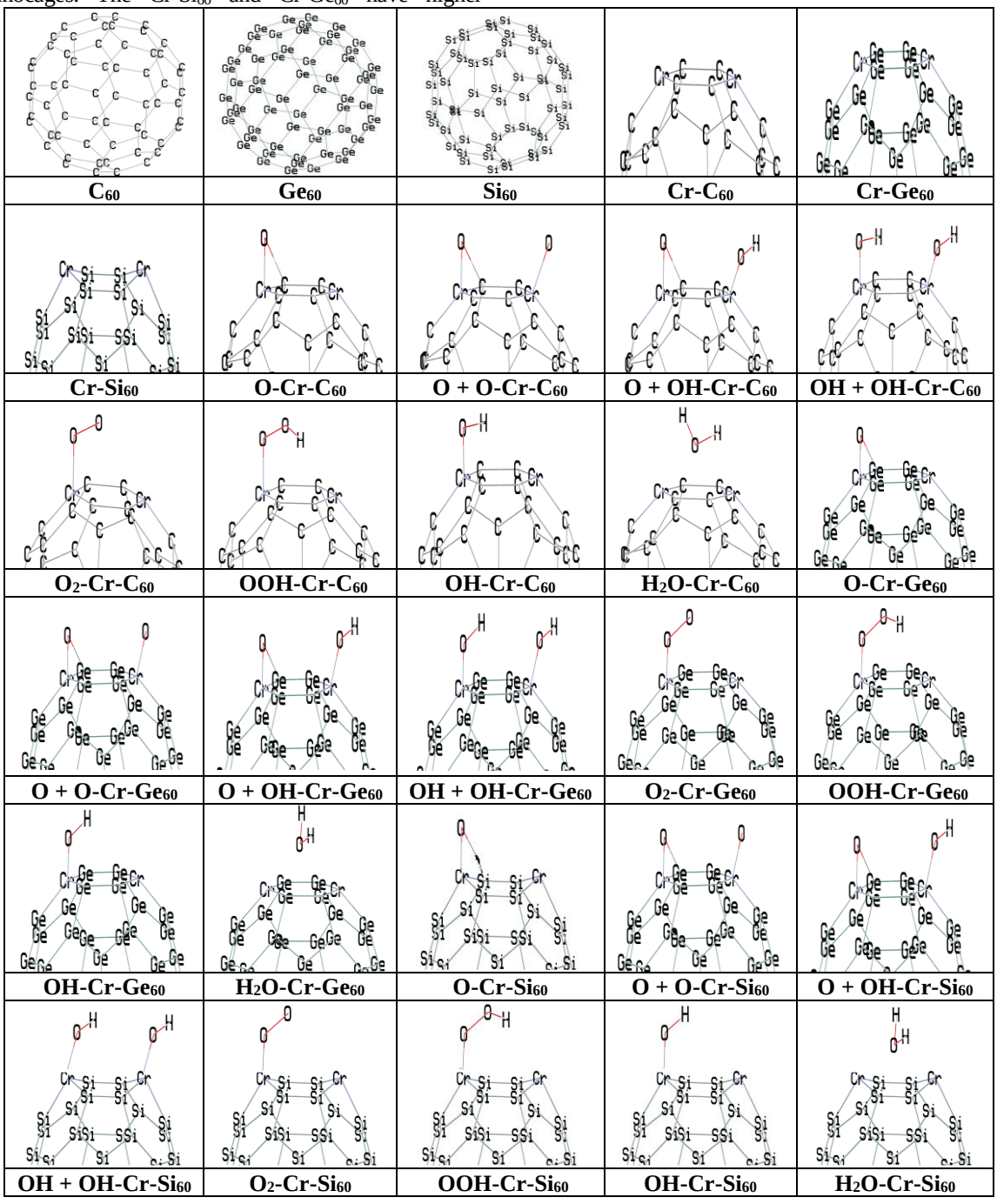

Fig. 1: Structures of Si_{60}, C_{60} and Ge_{60} nanocages, Cr doped nanocages (Cr-Si_{60}, Cr-C_{60} and Cr-Ge_{60}) and complexes with ORR species.

Table-1: The $E_{activation}$ and $\Delta G_{reaction}$ in eV for ORR on Cr-Si_{60}, Cr-C_{60} and Cr-Ge_{60} nanocages.

M06-2X/6-311+G (2d, 2p) model in gas phase						
Nanocages	**Cr-C_{60}**		**Cr-Ge_{60}**		**Cr-Si_{60}**	
ORR pathways 1, 2 and 3	**E_{act}**	**ΔG_{reac}**	**E_{act}**	**ΔG_{reac}**	**E_{act}**	**ΔG_{reac}**
surface-*O_2 → *O-surface-O*	**1.30**	**-1.52**	**1.34**	**-1.56**	**1.19**	**-1.74**
surface-*O_2 → surface-*OOH	**0.44**	**-1.39**	**0.45**	**-1.42**	**0.40**	**-1.58**
surface-*OOH → surface-O*	**1.12**	**-2.68**	**1.14**	**-2.75**	**1.02**	**-3.06**
surface-O* → surface-*OH	**1.05**	**-1.70**	**1.08**	**-1.74**	**0.96**	**-1.94**
surface-*OH → surface + H_2O	**0.66**	**-0.60**	**0.67**	**-0.62**	**0.60**	**-0.69**
surface-*OOH → HO*-surface-*OH	**1.55**	**-3.38**	**1.59**	**-3.46**	**1.42**	**-3.85**
HO*-surface-*OH → surface-*OH + H_2O	**0.96**	**-1.81**	**0.98**	**-1.86**	**0.87**	**-2.07**
surface-*OOH → HO*-surface-O*	**1.01**	**-1.17**	**1.04**	**-1.20**	**0.93**	**-1.34**
HO*-surface-O* → surface-O* + H_2O	**1.13**	**-1.45**	**1.15**	**-1.49**	**1.02**	**-1.66**
surface-O* → surface-*OH	**1.05**	**-1.69**	**1.08**	**-1.73**	**0.96**	**-1.93**
B3LYP/6-311+G (2d, 2p) model in gas phase						
Nanocages	**Cr-C_{60}**		**Cr-Ge_{60}**		**Cr-Si_{60}**	
ORR pathways 1, 2 and 3	**E_{act}**	**ΔG_{reac}**	**E_{act}**	**ΔG_{reac}**	**E_{act}**	**ΔG_{reac}**
surface-*O_2 → *O-surface-O*	**1.33**	**-1.49**	**1.37**	**-1.52**	**1.22**	**-1.70**
surface-*O_2 → surface-*OOH	**0.45**	**-1.36**	**0.46**	**-1.39**	**0.41**	**-1.54**
surface-*OOH → surface-O*	**1.15**	**-2.62**	**1.17**	**-2.69**	**1.04**	**-2.99**
surface-O* → surface-*OH	**1.07**	**-1.66**	**1.10**	**-1.70**	**0.98**	**-1.90**
surface-*OH → surface + H_2O	**0.68**	**-0.59**	**0.69**	**-0.61**	**0.61**	**-0.67**
surface-*OOH → HO*-surface-*OH	**1.59**	**-3.30**	**1.63**	**-3.38**	**1.45**	**-3.76**
HO*-surface-*OH → surface-*OH + H_2O	**0.98**	**-1.77**	**1.00**	**-1.82**	**0.89**	**-2.02**
surface-*OOH → HO*-surface-O*	**1.03**	**-1.14**	**1.06**	**-1.17**	**0.95**	**-1.31**
HO*-surface-O* → surface-O* + H_2O	**1.16**	**-1.42**	**1.18**	**-1.46**	**1.04**	**-1.62**
surface-O* → surface-*OH	**1.07**	**-1.65**	**1.10**	**-1.69**	**0.98**	**-1.89**
COSMO model in water						
Nanocages	**Cr-C_{60}**		**Cr-Ge_{60}**		**Cr-Si_{60}**	
ORR pathways 1, 2 and 3	**E_{act}**	**ΔG_{reac}**	**E_{act}**	**ΔG_{reac}**	**E_{act}**	**ΔG_{reac}**
surface-*O_2 → *O-surface-O*	**1.27**	**-1.55**	**1.31**	**-1.60**	**1.16**	**-1.78**
surface-*O_2 → surface-*OOH	**0.43**	**-1.42**	**0.44**	**-1.45**	**0.39**	**-1.62**
surface-*OOH → surface-O*	**1.09**	**-2.74**	**1.11**	**-2.81**	**1.00**	**-3.13**
surface-O* → surface-*OH	**1.03**	**-1.74**	**1.06**	**-1.78**	**0.94**	**-1.98**
surface-*OH → surface + H_2O	**0.65**	**-0.61**	**0.65**	**-0.63**	**0.59**	**-0.71**
surface-*OOH → HO*-surface-*OH	**1.52**	**-3.46**	**1.55**	**-3.54**	**1.39**	**-3.94**
HO*-surface-*OH → surface-*OH + H_2O	**0.94**	**-1.85**	**0.96**	**-1.90**	**0.85**	**-2.12**
surface-*OOH → HO*-surface-O*	**0.99**	**-1.20**	**1.02**	**-1.23**	**0.91**	**-1.37**
HO*-surface-O* → surface-O* + H_2O	**1.10**	**-1.48**	**1.12**	**-1.52**	**1.00**	**-1.70**
surface-O* → surface-*OH	**1.03**	**-1.73**	**1.06**	**-1.77**	**0.94**	**-1.97**

Reaction steps of ORR pathways on Cr-Si_{60}, Cr-C_{60} and Cr-Ge_{60} nanocages

The $E_{activation}$ and $\Delta G_{reaction}$ of reactions of pathways ORR on Cr-Si_{60}, Cr-C_{60} and Cr-Ge_{60} is examined [22]. The ΔG of reaction of ORR on Cr-Si_{60}, Cr-C_{60} and Cr-Ge_{60} is calculated:

$$\Delta G = \Delta H - T\Delta S + \Delta G_U + \Delta G_{pH} \quad (4)$$

The $\Delta G_U = -neU$, n is electron numbers and U is electrode potential.

The $E_{activation}$ of reactions of ORR on Cr-Si_{60}, Cr-C_{60} and Cr-Ge_{60} is calculated:

$$E_{activation} = E_{TS} - E_{IS} \quad (5)$$

The E_{TS} and E_{IS} are total energy of transition state and initial sate of reaction steps of ORR on Cr-Si_{60}, Cr-C_{60} and Cr-Ge_{60}. The HMO-LUMO gap energy (E_{HLG}) and charge transfer (q) for Cr-Si_{60}, Cr-C_{60} and Cr-Ge_{60} nanocages and complexes of ORR species with Cr-Si_{60}, Cr-C_{60} and Cr-Ge_{60} nanocages are calculated.

$$E_{HLG} = E_{HOMO} - E_{LUMO} \quad (6)$$

The E_{HOMO} and E_{LUMO} are energy of HOMO and LUMO of Cr-Si_{60}, Cr-C_{60} and Cr-Ge_{60} nanocages and complexes of ORR species with Cr-Si_{60}, Cr-C_{60} and Cr-Ge_{60} nanocages.

The adsorption of OOH on Cr-Si_{60}, Cr-C_{60} and Cr-Ge_{60} nanocages has higher $E_{adsorption}$ than O_2 adsorption. The dissociation of O_2 on Cr-Si_{60}, Cr-C_{60} and Cr-Ge_{60} nanocages has high $E_{activation}$ values. The dissociation of O_2 molecules on Cr-Si_{60}, Cr-C_{60} and Cr-Ge_{60} to O + O have high $E_{activation}$. The hydrogen atom can react by OOH on Cr-Si_{60}, Cr-C_{60} and Cr-Ge_{60} nanocages and the OOH adsorption on Cr-Si_{60}, Cr-C_{60} and Cr-Ge_{60} nanocages is more favorable process than O_2 dissociation.

In mechanism 1, the *OOH on Cr-Si_{60}, Cr-C_{60} and Cr-Ge_{60} is hydrogenated and H_2O is released and *O on Cr-Si_{60}, Cr-C_{60} and Cr-Ge_{60} is produced. The *O on Cr-Si_{60}, Cr-C_{60} and Cr-Ge_{60} is hydrogenated and *OH on Cr-Si_{60}, Cr-C_{60} and Cr-Ge_{60} is formed. The *OH on Cr-Si_{60}, Cr-C_{60} and Cr-Ge_{60} is

hydrogenated and H_2O is separated. The $\Delta G_{reaction}$ of creation of the second H_2O on Cr-Si_{60}, Cr-C_{60} and Cr-Ge_{60} nanocages are -0.69, -0.60 and -0.62 eV. In pathway 2, the *OOH on Cr-Si_{60}, Cr-C_{60} and Cr-Ge_{60} is hydrogenated and HO*-*OH and -*OH are formed and H_2O is released. In final step, the *OH on Cr-Si_{60}, Cr-C_{60} and Cr-Ge_{60} nanocages is hydrogenated and H_2O is released. The $E_{activation}$ of creation of the second H_2O on Cr-Si_{60}, Cr-C_{60} and Cr-Ge_{60} nanocages are 1.02, 1.13 and 1.15 eV. In mechanism 3, *OOH on Cr-Si_{60}, Cr-C_{60} and Cr-Ge_{60} is dissociated to *OH and *O. The *OH is hydrogenated and H_2O is formed on Cr-Si_{60}, Cr-C_{60} and Cr-Ge_{60}. The *O on Cr-Si_{60}, Cr-C_{60} and Cr-Ge_{60} is hydrogenated and*OH is formed. The *OH on Cr-Si_{60}, Cr-C_{60} and Cr-Ge_{60} is hydrogenated and $E_{activation}$ of creation of *OH on Cr-Si_{60}, Cr-C_{60} and Cr-Ge_{60} nanocages are 0.96, 1.05 and 1.08 eV.

In mechanisms 1, 2 and 3 the formation of -*OH, creation of -*OH and H_2O and production of -*O and H_2O are rate-determining steps for ORR on Cr-Si_{60}, Cr-C_{60} and Cr-Ge_{60}. The $\Delta E_{activation}$ of -*OH formation on Cr-Si_{60}, Cr-C_{60} and Cr-Ge_{60} 1 is lower than -*OH, -*O and H_2O in pathways 2 and 3. The $\Delta G_{reaction}$ of -*OH formation on Cr-Si_{60}, Cr-C_{60} and Cr-Ge_{60} 1 is higher than -*OH, -*O and H_2O in pathways 2 and 3. The pathway 1 is effective mechanisms for ORR on Cr-Si_{60}, Cr-C_{60} and Cr-Ge_{60}. The over-potential of ORR on Cr-Si_{60}, Cr-C_{60} and Cr-Ge_{60} are lower than metal-based catalysts. The Cr-Si_{60} and Cr-Ge_{60} nanocages have lower over-poential for ORR than Cr-C_{60} nanocage. The Cr-Si_{60} and Cr-Ge_{60} nanocages are catalyzed the ORR with high efficiency.

Table-2: The over-potential in V, E_{HLG} in eV and q in *e* of complexes of Cr-Si_{60}, Cr-C_{60} and Cr-Ge_{60} with ORR species.

M06-2X/6-311+G (2d, 2p) model in gas phase						
	Cr-C_{60}		**Cr-Ge_{60}**		**Cr-Si_{60}**	
Complexes	**E_{HLG} (eV)**	**q (e)**	**E_{HLG} (eV)**	**q (e)**	**E_{HLG} (eV)**	**q (e)**
O-nano	**-4.30**	**-0.23**	**-3.84**	**-0.26**	**-3.34**	**-0.30**
O-nano-O	**-2.13**	**-0.47**	**-1.90**	**-0.53**	**-1.66**	**-0.60**
O-nano-OH	**-2.42**	**-0.41**	**-2.16**	**-0.46**	**-1.88**	**-0.53**
HO-nano-OH	**-2.49**	**-0.40**	**-2.22**	**-0.45**	**-1.93**	**-0.52**
O_2-nano	**-3.37**	**-0.03**	**-3.01**	**-0.03**	**-2.62**	**-0.04**
HOO-nano	**-4.42**	**-0.11**	**-3.94**	**-0.13**	**-3.43**	**-0.15**
HO-nano	**-4.65**	**-0.22**	**-4.15**	**-0.24**	**-3.61**	**-0.28**
H_2O-nano	**-3.29**	**-0.02**	**-2.94**	**-0.02**	**-2.55**	**-0.02**
Nanocages	**Cr-Si_{60}**		**Cr-C_{60}**		**Cr-Ge_{60}**	
Over-potential	**0.25**		**0.29**		**0.33**	
B3LYP/6-311+G (2d, 2p) model in gas phase						
	Cr-C_{60}		**Cr-Ge_{60}**		**Cr-Si_{60}**	
Complexes	**E_{HLG} (eV)**	**q (e)**	**E_{HLG} (eV)**	**q (e)**	**E_{HLG} (eV)**	**q (e)**
O-nano	**-4.11**	**-0.22**	**-3.67**	**-0.25**	**-3.19**	**-0.29**
O-nano-O	**-2.04**	**-0.45**	**-1.82**	**-0.50**	**-1.58**	**-0.58**
O-nano-OH	**-2.31**	**-0.39**	**-2.07**	**-0.44**	**-1.80**	**-0.51**
HO-nano-OH	**-2.38**	**-0.38**	**-2.12**	**-0.43**	**-1.85**	**-0.50**
O_2-nano	**-3.23**	**-0.03**	**-2.88**	**-0.03**	**-2.50**	**-0.04**
HOO-nano	**-4.22**	**-0.11**	**-3.77**	**-0.12**	**-3.28**	**-0.14**
HO-nano	**-4.45**	**-0.21**	**-3.97**	**-0.23**	**-3.45**	**-0.26**
H_2O-nano	**-3.15**	**-0.01**	**-2.81**	**-0.02**	**-2.44**	**-0.02**
Nanocages	**Cr-Si_{60}**		**Cr-C_{60}**		**Cr-Ge_{60}**	
Over-potential	**0.23**		**0.27**		**0.31**	
COSMO model in water						
	Cr-C_{60}		**Cr-Ge_{60}**		**Cr-Si_{60}**	
Complexes	**E_{HLG} (eV)**	**q (e)**	**E_{HLG} (eV)**	**q (e)**	**E_{HLG} (eV)**	**q (e)**
O-nano	**-4.50**	**-0.24**	**-4.01**	**-0.27**	**-3.49**	**-0.31**
O-nano-O	**-2.23**	**-0.49**	**-1.99**	**-0.55**	**-1.73**	**-0.63**
O-nano-OH	**-2.53**	**-0.43**	**-2.26**	**-0.48**	**-1.96**	**-0.56**
HO-nano-OH	**-2.60**	**-0.42**	**-2.32**	**-0.47**	**-2.02**	**-0.54**
O_2-nano	**-3.53**	**-0.03**	**-3.15**	**-0.03**	**-2.74**	**-0.04**
HOO-nano	**-4.62**	**-0.12**	**-4.12**	**-0.13**	**-3.58**	**-0.15**
HO-nano	**-4.86**	**-0.22**	**-4.34**	**-0.25**	**-3.77**	**-0.29**
H_2O-nano	**-3.44**	**-0.02**	**-3.07**	**-0.02**	**-2.67**	**-0.02**
Nanocages	**Cr-Si_{60}**		**Cr-C_{60}**		**Cr-Ge_{60}**	
Over-potential	**0.26**		**0.28**		**0.32**	

Conclusion

In this work, the ORR mechanisms on Cr-Si_{60}, Cr-C_{60} and Cr-Ge_{60} nanocages are investigated. The Cr atoms of Cr-Si_{60}, Cr-C_{60} and Cr-Ge_{60} are active positions to adsorb the ORR species. The adsorption OOH on Cr-Si_{60}, Cr-C_{60} and Cr-Ge_{60} nanocages has higher $E_{adsorption}$ than O_2 adsorption and dissociation of O_2 molecules on Cr-Si_{60}, Cr-C_{60} and Cr-Ge_{60} nanocages has high $E_{activation}$ values. The ORR on Cr-Si_{60}, Cr-C_{60} and Cr-Ge_{60} nanocages is processed by three pathways. The $\Delta E_{activation}$ of -*OH formation on Cr-Si_{60}, Cr-C_{60} and Cr-Ge_{60} 1 is lower than -*OH, -*O and H_2O in pathways 2 and 3. The Cr-Si_{60}, Cr-C_{60} and Cr-Ge_{60} have higher catalytic activity for ORR processes than metal-based catalysts and AlN, C, BN, AlP and BP nanocages and AlN, C, BN, Si, Ge, AlP and BP nanotubes**.** The $\Delta G_{reaction}$ of -*OH formation on Cr-Si_{60}, Cr-C_{60} and Cr-Ge_{60} 1 is higher than -*OH, -*O and H_2O in pathways 2 and 3. The pathway 1 is acceptable mechanism for ORR on Cr-Si_{60}, Cr-C_{60} and Cr-Ge_{60}. The over-potential of ORR on Cr-Si_{60}, Cr-C_{60} and Cr-Ge_{60} are lower than metal-based catalysts. The Cr-Si_{60} and Cr-Ge_{60} nanocages are proposed to catalyze the ORR with high efficiency.

Acknowledgement:

Jilin Provincial Department of Education Scientific Research Project, No: JJKH20230423KJ.

References

1. Z. L. Zhao, Q. Wang, L. Zhang, H. M. An, L. Zhou, M. L. Chang, Galvanic exchange-formed ultra-low Pt loading on synthesized unique porous Ag-Pd nanotubes for increased active sites toward oxygen reduction reaction, *Electrochim. Acta*, **263**, 209 (2018).
2. J. Yao, C. Li, K. Sun, Y. Cai, H. Li, W. Ouyang, H. Li, Ndc-scene: Boost monocular 3d semantic scene completion in normalized device coordinates space. *IEEE/CVF Int. Computer Vision* **11**, 9455 (2023).
3. P. Li, J. Abbas, D. Balsalobre-Lorente, Q. Wang, Q. Zhang, S. A. R. Shah, Impact of sectoral mix on environmental sustainability: How is heterogeneity addressed? *Gondwana Res.* **128**, 86 (2024).
4. J. X. Chen, L. Peng, J. Ma, H. P. Ying, Liberation of a pinned spiral wave by a rotating electric pulse. *Euro. phys. Lett.*, **107**, 38001 (2014).
5. X. Sun, S. Zhu, J. Guo, S. Peng, X. Qie, Z. Yu, P. Li, Exploring ways to improve China's ecological well-being amidst air pollution challenges using mixed methods. *J. Environ. Management*, **364**, 121457 (2024).
6. M. M. Khotbehsara, M. Zadshir, B. M. Miyandehi, E. Mohseni, S. Rahmannia, S. Fathi, Rheological, mechanical and durability properties of self-compacting mortar containing nano-TiO2 and fly ash. *J. American Sci.*, **10**, 222 (2014).
7. B. Mehdizadeh, K. Vessalas, B. Ben, A. Castel, S. Deilami, H. Asadi, Advances in Characterization of Carbonation Behavior in Slag-Based Concrete Using Nanotomography. *Int. Variability*, **1**, 297 (2022).
8. B. Mehdizadeh Miyandehi, K. Vessalas, A. Castel, M. Mortazavi, Investigation of Carbonation Behaviour in High-Volume GGBFS Concrete for Rigid Road Pavements. *ASCP* **1**, 12 (2023).
9. A. Naseri, B. Maleki, T. Asheghi Mehmandari, A. Tohidi, A. Fahimifar, Investigating the influence of Sample geometric variations on mechanical characterization in rock and concrete. *J. Mining Environ.*, **16**, 1089 (2025).
10. P. Jafari, E. Rasekh, T. Asheghi Mehmandari, M. Mohammadifar, A. Fahimifar, D. Jahed Armaghani, Upper-bound solutions for active face failure in shallow rectangular tunnels in anisotropic and non-homogeneous undrained clays. *Geotech. Geolog. Eng.*, **43**, 1 (2025).
11. T. A. Mehmandari, M. Shokouhian, M. Imani, A. Fahimifar, Experimental and numerical analysis of tunnel primary support using recycled, and hybrid fiber reinforced shotcrete. *In Structures*, **63**, 106282 (2024).
12. Mehmandari, T. A., Shokouhian, M., Imani, M., Tee, K. F., Fahimifar, A. Split Tensile Behavior of Recycled Steel Fiber-Reinforced Concrete. *ACI Mat. J.*, **122**, 5147 (2025).
13. T. A. Mehmandari, M. Shokouhian, M. Z. Josheghan, S. A. Mirjafari, A. Fahimifar, D. J. Armaghani, K. F. Tee, Flexural properties of fiber-reinforced concrete using hybrid recycled steel fibers and manufactured steel fibers. *J. Building Eng.*, **98**, 111069 (2024).
14. T. A. Mehmandari, D. Mohammadi, M. Ahmadi, M. Mohammadifar, Fracture mechanism and ductility performances of fiber reinforced shotcrete under flexural loading insights from digital image correlation (DIC). *Insight Civil Eng.*, **7**, 611 (2024).
15. M. Ershadi, M. Javanbakht, D. Brandell, S. A. Mozaffari, A. M. Aghdam, Facile synthesis of amino-functionalized mesoporous Fe3O4/rGO 3D nanocomposite by diamine compounds as Li-ion battery anodes. *Appl. Sur. Sci.*, **601**, 154120 (2022).

16. A. Molaei Aghdam, S. Habibzadeh, M. Javanbakht, M. Ershadi, M. R. Ganjali, High interspace-layer manganese selenide nanorods as a high-performance cathode for aqueous zinc-ion batteries. *ACS Appl. Energy Mat.*, **6**, 3225 (2023).
17. A. Molaei Aghdam, N. Mikaeili Chahartagh, E. Delfani, High-Efficient Capacitive Deionization Using Amine-Functionalized ZIF-67@2D MXene: Toward Ultrahigh Desalination Performance. *Adv. Mat. Techn.*, **8**, 2300628 (2023).
18. A. M. Aghdam, N. M. Chahartagh, S. Namvar, M. Ershadi, F. B. Ajdari, E. Delfani, Improving the performance of a SnS 2 cathode with interspace layer engineering using a Na+ insertion/extraction method for aqueous zinc ion batteries. *J. Mat. Chem. A*, **12**, 1047 (2024).
19. F. B. Ajdari, F. Abbasi, A. M. Aghdam, F. G. C. Khaneh, A. G. Arjenaki, V. Farzaneh, S. Ramakrishna, Innovative self-repairing binders tackling degradation and de-lithiation challenges: Structure, mechanism, high energy and durability. *Mat. Sci. Eng. Reports*, **160**, 100830 (2024).
20. Y. Ru, M. Gruninger, Y. Dou, Robust self-supervised symmetric nonnegative matrix factorization to the graph clustering. *Sci. Reports*, **15**, 7350 (2025).
21. Y. Huo, S. Gang, C. Guan, Fcihmrt: *Feature cross-layer interaction hybrid method based on Res2Net and transformer for remote sensing scene classification, Electronics*, **12**, 4362 (2023).
22. J. Singh, R. Abraham, Magnetic Catalyst CdFe2O4: Direct Conversion of Thiols into Antibacterial Sulfonamides. *Biol. Mol. Chem.*, **2**, 13 (2024).